Department of
Aerospace Engineering -
University of Michigan
Ann Arbor, MI, 48014
(734) 904-1094

Darren Schumacher, Vice President - Technology and Innovation
Stoneridge, Inc.
39675 MacKenzie Drive, Suite 400
Novi, Michigan, 48377

Subject: Final Report for Optimization of MirrorEye™ Camera System For Trucks and Buses

Dear Mr. Schumacher,

Enclosed is our report for the study of an optimized design for the MirrorEye™ Camera system used on trucks and buses. Included in this report is the optimization of both the aerodynamic properties of the system, as well as a method for the reduction of camera soiling.

This final report outlines our findings in using a combination of computational fluid dynamics (CFD) and physical testing to research a proper aerodynamic design, as well as our methods to decrease soiling of the camera. The use of CFD and wind tunnel testing has allowed us to produce an aerodynamically efficient prototype design of the camera system. A testing appartus was also produced in order to characterize a reduction in soiling. We are pleased to confidently present our discoveries by our project deadline of December 13, 2019 with our team of five engineers.

Thank you for offering us the opportunity to work with you in order to reach a high quality solution to this unique problem. We appreciate your continued support through our research and look forward to potentially continuing our work with you in the future.

Sincerely,

Andrew Caulkins Garrett Duckworth Drake Rundell

Alexander Schwedt Noah Springer

Final Report:

Optimization of MirrorEye™ Camera System for Trucks and Buses

MirrorEye™
the future in truck mirror replacement

MICHIGAN ENGINEERING
UNIVERSITY OF MICHIGAN

Final Report:

Optimization of MirrorEye™ Camera System for Trucks and Buses

December 13, 2019

Prepared by:

All Eyes on MirrorEye™
Andrew Caulkins
Garrett Duckworth
Drake Rundell
Alexander Schwedt
Noah Springer

Prepared for:

Stoneridge, Inc.
Darren Schumacher, Vice President Technology and Innovation
Luis Bernal, Lead Liaison
Tim Smith, Technical Supervisor
Jack Fishstrom, Communications Manager

Contents

I List of Figures

II List of Tables

III List of Equations

IV Nomenclature

ρ	=	Density	...	[kg/m^3]
P	=	Pressure	...	[kg/m·s^2]
R	=	Specific Gas Constant	...	[287.05 J/kg·K]
T	=	Temperature	...	[K]
A	=	Planform Area	...	[m^2]
V	=	Free-stream Velocity	...	[m/s]
C_D	=	Coefficient of Drag	...	[dimensionless]
μ	=	Dynamic Viscosity	...	[kg/m·s]
b	=	Sutherland Constant #1	...	[1.458×10^{-6} kg/m·s·$\sqrt{K}$]
S	=	Sutherland Constant #2	...	[110.4 K]
Re	=	Reynold's Number	...	[dimensionless]
L	=	Characteristic Length	...	[m]
AD	=	Average Difference in Percent Reduction of Soiling	...	[dimensionless]

1 Executive Summary

The MirrorEye™ camera system was designed to replace conventional side mirrors on large trucks and buses to help decrease fuel costs for operators and increase overall safety on the road. Our group was tasked with optimizing this system through a redesign of the housing unit, which is mounted to the side of the vehicle, and the implementation of an soiling reduction system that would lower the soiling of the camera lens, further enhancing visibility and safety. Criteria was set and met for these two independent tasks through a series of testing at the University of Michigan, rendering our work a success. This report includes details of our criteria, testing methods, data acquisition and analysis, alternatives, conclusions, costs, project schedule, and future efforts to further optimize this system.

Our work was building off of a previous student team who had similar tasks, which made our goal to take their work and further enhance the MirrorEye™ product. Our criteria was to decrease the coefficient of drag by 20% from the previous group's model and develop a system that could reliably remove debris from the camera lenses. This criteria was met through a series of 5' x 7' wind tunnel testing on our 3D printed model and the creation of a soiling reduction sub-system. Our final camera system model yielded a coefficient of drag value of 0.32, a **42%** decrease from the previous model. The soiling reduction sub-system yielded a soiling decrease of **64%**. These systems can be modified to the manufacturing specifications of Stoneridge, Inc. for application onto vehicles. Moving forward, we recommend that these two systems be integrated together for application, in addition to further optimization efforts.

2 Introduction

The MirrorEye™ camera system, produced by Orlaco, a subsidiary of Stoneridge Inc., was designed to replace traditional side mirrors on trucks and buses to improve fuel efficiency and safety. The University of Michigan is working with Orlaco to help optimize the design of the system. Using the available resources at the University, we were tasked with producing this design optimization. The redesign would further increase the efficiency of the camera system and decrease the amount of soiling on the camera lens in order to increase fuel efficiency and enhance safety of large vehicles. The optimization was completed in conjunction with research of similar camera systems on vehicles. The background, statement of the problem, potential impacts of the optimization, previous work, our thesis, and a review of some previous literature for this problem are described below.

2.1 Background

Orlaco has developed the MirrorEye™ camera system that can be installed on large trucks and buses in place of side mirrors, reducing the overall drag and increasing fuel economy. The company has been working with the College of Engineering at the University of Michigan to help optimize the system since January 2019. Our mission is to further optimize the system; our main focal points being to further reduce the drag of the system and reduce the soiling of the camera lenses during operation due to accretion of dirt and other substances which impair visibility. Our objective was to characterize the aerodynamic forces produced by the current design, particularly drag, compare them to a number of new designs in a Computational Fluid Dynamics (CFD) program, and then advance to real world testing using the available wind tunnels at the University. We also found that soiling is coupled to the aerodynamics of the body and thus our design could produce or exacerbate the issue. We developed a quantitative system to measure the level of soiling and tested a number of passive and active anti-soiling systems. These experiments were conducted at the University of Michigan, Ann Arbor, on North Campus spanning from October 2019 to December 2019.

2.2 Statement of Problem

Side impact crashes from large trucks and buses result in hundreds of millions of dollars worth of damage and dozens of fatalities every year [1]. MirrorEye™ camera systems were designed to replace side mirrors to reduce the rate at which these incidents occur and increase the fuel efficiency of these vehicles. These systems are commercially available, but are not currently in widespread use as they present their own disadvantages. The main disadvantage is that the camera lens is subject to soiling; the accretion of dirt or other material on the optics which reduce visibility. A soiled lens renders the system less effective and creates a more hazardous situation than what would be had with a traditional side mirror. By reducing the soiling and increasing the aerodynamic advantages, the MirrorEye™ system will consistently save more lives on the road and save operators money. This, in turn, will make the product more profitable for Stoneridge Inc., leading them to potentially become a household name in the trucking and busing industries.

2.3 Impact and Effect

With the goal of the project being on characterization and optimization of the MirrorEye™ camera system, the impacts will be felt mainly by the shipping industry, the main operators of the class of vehicles these systems would support. The benefits include a reduction in the amount of fuel costs per year due to decreased drag and enhanced vision for the driver, leading to a safer driving environment. Totaling about 57% of the worlds freight transportation, trucks use an average of about 22 quadrillion Btu of energy (approximately a fifth of the United State's annual energy consumption) in the transportation industry [2]. The current design reduces energy usage of a vehicle by 2-3%, and our design could make these improvements even greater. The second benefit is to improve the safety of the vehicle for both the driver of the truck and those who are in proximity to it. Trucks are inherently more likely to get into side swipe accidents[1]. The MirrorEye™ system is meant to actively prevent and reduce these types of accidents to help save countless lives every year.

2.4 History

Our group is the continuation of a previous University of Michigan student group that worked on the MirrorEye™ camera system problem in the Winter of 2019. However, this group focused mainly on the aerodynamic portion of the design and obtained only small reductions in soiling because of the design itself, rather than addressing soiling as a separate task.

2.5 Task

Our team was tasked to further increase the aerodynamics of the MirrorEye™ design and to create a system that would reduce soiling of the camera lenses. Our goals for these two problems were to achieve a 20% reduction in the coefficient of drag from the previous group's design and to create a system where the camera lenses is not subject to the effects of soiling, whether through a passive or active cleansing system. We also strived to create a design with a cutting-edge appeal, much like the technology, in the physical appearance of the model as we realize attractiveness to customers inherently enhances market value.

2.6 Thesis

These problems can be addressed by furthering from what was completed last year by producing a design that is more aerodynamically efficient, while also being more appealing to the eye than a simple airfoil. The soiling would be addressed by implementing a self-cleaning lens, along with material that stops debris from sticking to the lens.

2.7 Literature

Formal work on the development of the new system was based off of research on how similar systems fix these unique problems. For aerodynamics, knowledge from previous coursework at the University of Michigan aided in obtaining an understanding of the general design. For soiling, we looked into how other cameras address debris interactions and how viewing screens are kept clear in a low visibility environment. Widely used methods for image analysis and comparison based on blurriness were researched in order to quantify results in soiling reduction. Access to the previous group's data and research is also available for reference and as a potential stepping stone.

3 Criteria

To prove our thesis we deemed it important to determine and analyze two major criteria to focus on in the development of our systems. The two major criteria have been selected to guide our research into the improved aerodynamics and self-cleaning camera system:

- **Reduction of the Drag Coefficient by 20%**
  - Focusing on the drag coefficient allows for the direct scaling of a prototype design to full-scale through the use of a non-dimensional parameter. The coefficient of drag is dependent only on geometry and is independent of size of the object and the conditions it operates in. As such, any errors in scaling from our models to the production model of the MirrorEye™ camera would still net a performance increase in terms of drag.
  - To decrease the coefficient of drag, we started with several entirely new designs with a focus on aerodynamic efficiency. To verify our designs decreased the coefficient of drag, we completed computational fluid dynamic (CFD) simulations on the newly designed systems, and then proceeded with the lowest coefficient of drag model found through the simulations. The leading model was selected for further testing in the 5' x 7' wind tunnel.
- **Create a System that can Consistently Reduce Soiling**
  - The decrease of soiling of the system using an active or passive method must be repeatable on all scales from prototype to production. Such a system should operate as efficiently as possible on all levels of required size. A passive system, assuming the same geometry, should have the same flow characteristics at all sizes and therefore amass the same amount of debris. For an active system, as long as the system is applicable to the geometry, it can actively counteract the build up of debris on the lens.
  - The effectiveness of our self-cleaning camera system to remove debris and liquid from the lens requires the soiling amount, or rather its effect on an image, to be numerically quantified. A procedure for this quantification will provide a method of measurement in which we can base the performance of our system on. This system allows us to provide a repeatable and independent method to quantify soiling, rather than subjective and qualitative testing done by a person. The implementation of the technique will take place using a camera system with real time image analysis.

4 Methods

The following section classifies the methods and procedures taken to conduct the experiments for the aerodynamic and soiling reduction testing, as well as stylistic improvement. It also outlines the assumptions and theories for each section and the production and simulation of the models, if applicable. The construction of the models and supporting equipment is also included.

4.1 Aerodynamic Optimization and Characterization

Outlined below are the methods used to optimize the aerodynamic design of our MirrorEye™ model. Each characterization includes the assumptions made and the simulation and experimentation methods.

4.1.1 Assumptions and Theories

As the MirrorEye™ camera is a complex shape (i.e. it is not an airfoil), the theories that were applied are from basic aerodynamics courses and observations for general shapes instead of a general theory for a specific simple shape. Therefore, we are restricted to numerical and real world testing to characterize designs. However, our design is bounded by the intention to operate exclusively at relatively low speeds, set to be at a minimum of 20 mph (9 m/s) and a maximum of 90 mph (41 m/s). As such, we can safely characterize the entire operating range of speeds without extrapolation.

The angle of attack is also fixed while in operation, though testing at non-zero angles was done in order to ensure the design angles were optimized. In the wind tunnel, we assumed that the drag force of the camera system was the difference in drag force of the system with the mount and the mount by itself. Since our analysis focused solely on the drag force, the maximum amount of lift is negligible (4.5 N) as are the side forces and moments.

4.1.2 Modeling and Simulation

We started with ten designs which were subjected to CFD modeling and simulation. These models were built using CAD (Computer-Aided Design) software. The initial designs were modeled and simulated in STAR-CCM+ and ANSYS to determine the most aerodynamic design. The design with the lowest simulated coefficient of drag was ultimately tested on small and full scale prototypes in both the 2’ x 2’ and 5’ x 7’ wind tunnels. Seen in *Figure 1* there are images of the final model we chose and an example simulation showing the streamlines around the design. In *Appendix A.1*, a detailed engineering schematic of the model has been included.

(a) Catia V5 Final Model

(b) Star CCM+ Streamline Simulation

Figure 1: Complete CAD model of the MirrorEye™ redesign with CFD analysis.

4.1.3 Construction of Models

The initial model of the design was produced in small-scale using a foam cutter, followed by a full-scale model created using a 3D printer in PLA plastic. The foam model was produced for 2' x 2' wind tunnel testing, to help verify our initial simulation data. The full-scale model was 3D printed along with an independent mount to be used in 5' x 7' wind tunnel testing. The data obtained from this full-scale testing was used to verify our thesis. Seen in *Figure 2* is the final physical model and test stand.

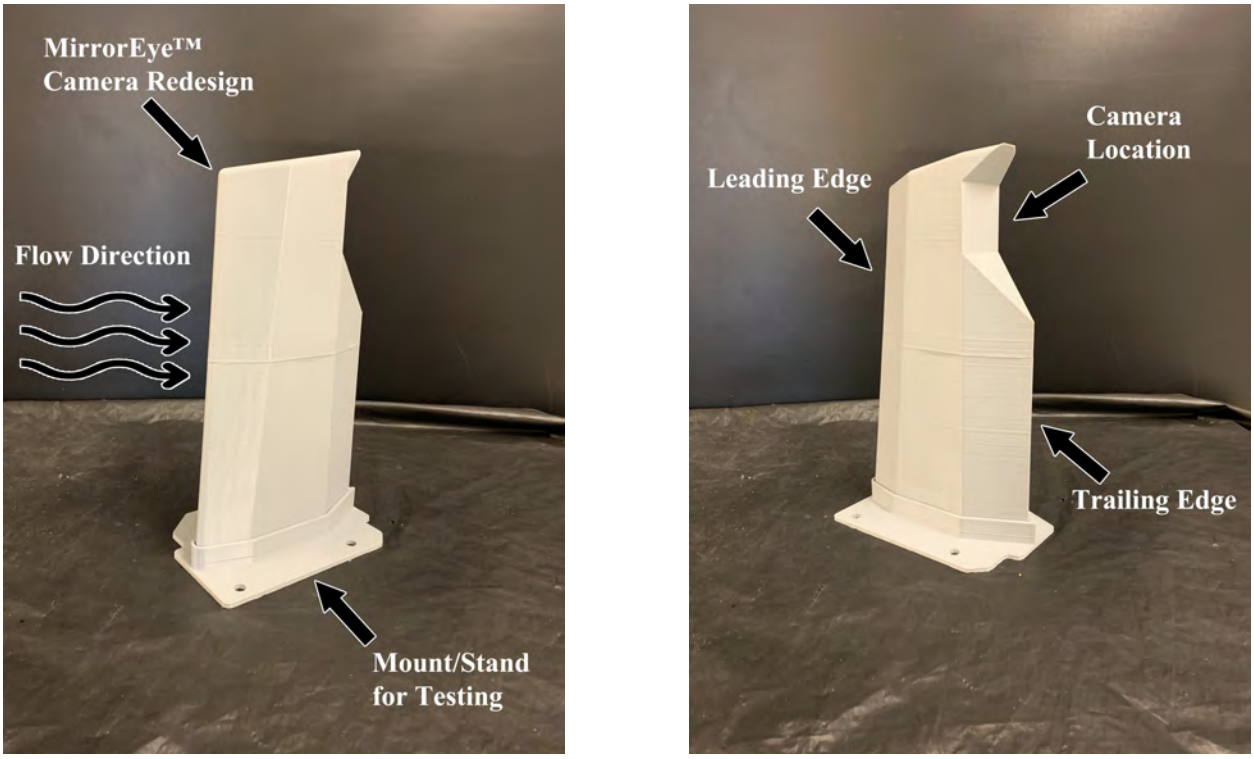

Figure 2: Redesigned MirrorEye™ physical model with mounting stand for testing and display produced with a 3D printer in PLA plastic.

4.1.4 Equipment & Apparatuses

The 5' x 7' wind tunnel was essential in the aerodynamic characterization of the design. Force balances connected to the mount of the model were used to measure the forces induced on the object in the wind tunnel. The mount and object sit in the wind tunnel and transfer their forces across the mount to strain gauges below. Mercury barometers and thermometers were utilized to find the atmospheric conditions while testing. An airspeed readout was viewable from outside the wind tunnel to ensure data points were correctly recorded. The velocity was confirmed with readings from a pressure board using gauge oil located near the wind tunnel. Seen in *Figure 3* is a schematic diagram of the 5' x 7' wind tunnel that was used for physical testing.

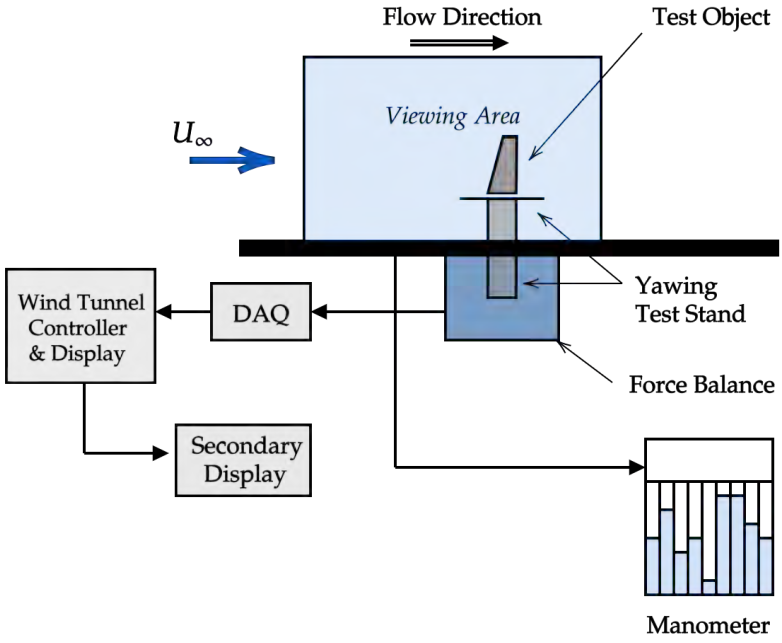

Figure 3: Schematic of 5' x 7' wind tunnel showing important features that were used during testing.

4.1.5 Setup, Calibration, and Procedure(s)

The camera system design, with mount, was initially fixed on the measuring balance located within the wind tunnel. Once the mounting plate is bolted in, it is aligned and calibrated as described in the analysis section below. The design is firmly fixed to the mount as the forces induced are expected to be non-negligible. A range of flow speeds from 20 mph to 90 mph were selected as these are the approximate airspeeds for trucks in highway conditions.

The wind tunnel was brought up to speed as reported by a digital pressure sensor and confirmed with a manual gauge oil reading. Temperature data for the flow was also recorded through the wind tunnel's DAQ system. Multiple data points were taken for each speed and recorded digitally before increasing to the next speed, repeating for all velocities. The wind tunnel was then brought back down to static conditions, the design was removed, and process was repeated for the mount alone. The data was recorded and interpreted as stated in the analysis section. The raw data is reported in *Appendix A.4* in the form of a table.

4.2 Soiling Reduction

The methods taken to develop a soiling reduction system with numerical characterization for the MirrorEye™ camera system lenses are detailed below.

4.2.1 Assumptions and Theories

For testing purposes, we assume zero air speed. The following assumption is valid as we are taking a static approach to the system and the testing of the system is solely dependent on the soiled percentage of the lens. If the system can accommodate for a soiled system at standstill, then we expect that in operation, there will be less soiling as there will not be full-on direct exposure to the elements. Therefore, if the system

can withstand excess soiling statically, we assume it can withstand normal exposure when in operation. Our testing apparatus is loosely based on the design of the clear view screen [3] which is implemented on naval ships to maintain visual clarity. We researched the design and made modifications in order to use the technique with a camera, while ensuring implementation on a small scale.

4.2.2 Equipment and Apparatuses

For our soiling reduction system, we developed a test stand that houses a Raspberry Pi board, a camera, and a motor. Our Raspberry Pi board allows for fast testing and extensive support for tertiary devices such as motors and cameras. *Figure 4* displays the testing apparatus with labels for the main components in connection with the computer.

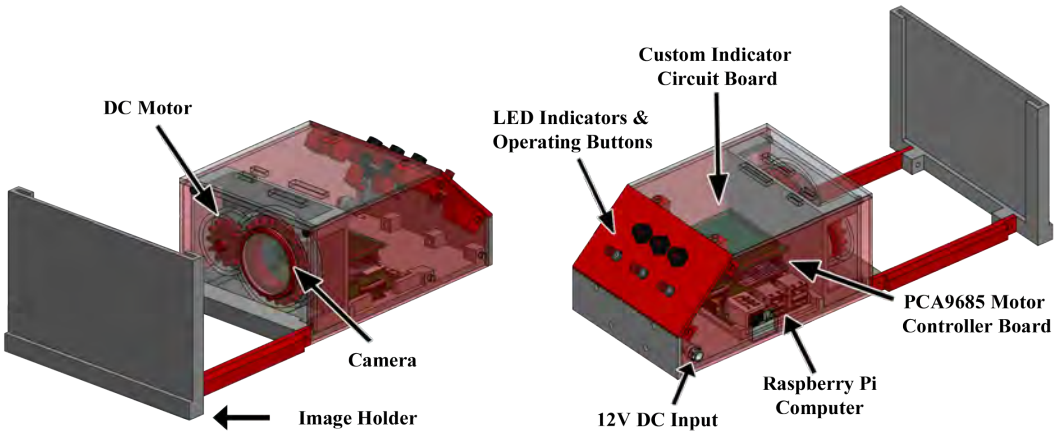

Figure 4: Major components of the test stand used for data collection in the testing of soiling reduction on the camera system.

Figure 5 is a flow diagram of how the system operates through the Raspberry Pi. The system can retrieve images from the camera, while also connecting to the controller boards and operating interface. Sof Sole Heavy-Duty Silicone Waterproofer was used as a hydrophobic spray in application on the testing lenses for various iterations. Details about the spray can be seen in *Appendix A.3*.

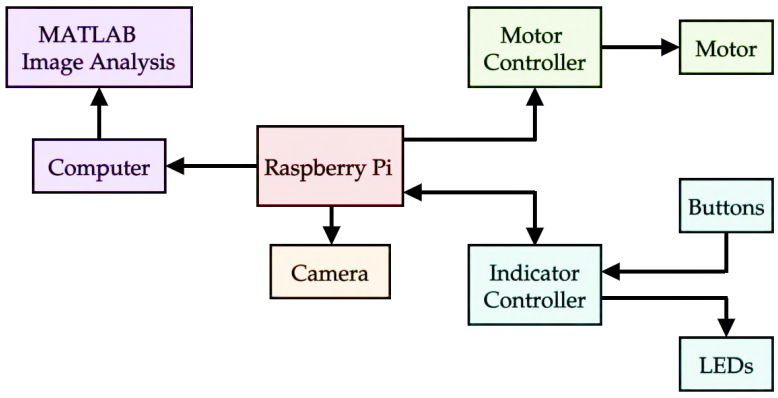

Figure 5: System overview of the test stand using for data collection in the testing of soiling reduction on the camera system.

4.2.3 Setup, Calibration, Procedure(s)

The testing was done in a controlled environment with steady and proper lighting. The calibration of this process was not needed as we were comparing results against each other and are normalized to themselves; these results would be used in determining the reduction in soiling of the system. Our procedure included a constant amount of sprays from a spray bottle, a constant operating time where the lens sitting in front of the camera is spun, and similar liquids used in each case. We tested both normal water and water with salt added to it to replicate possible particles suspended in the water. *Figure 6* is a diagram of the testing procedure..

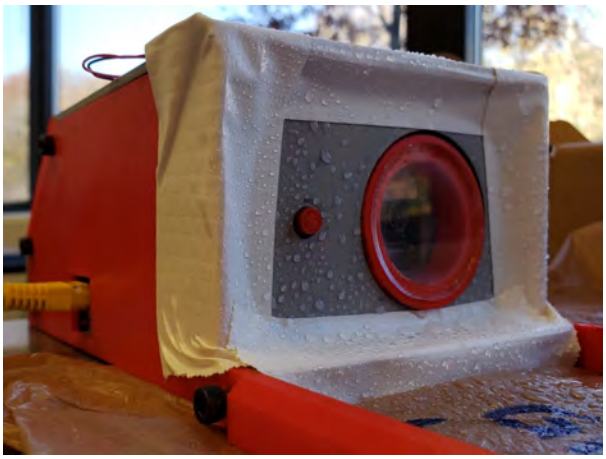

(a) Control Photo is Taken

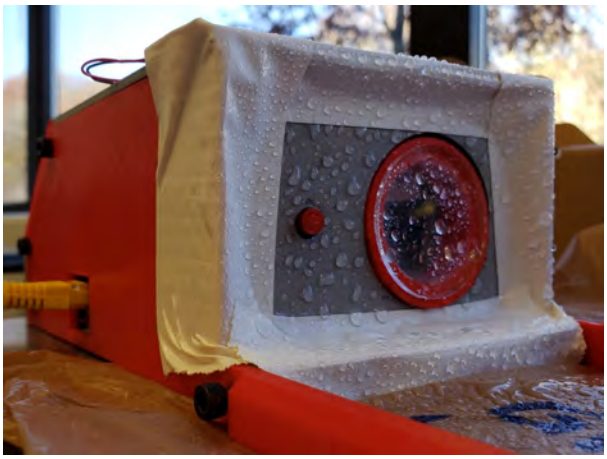

(b) Lens Sprayed 3 Times, Soiled Photo is Taken

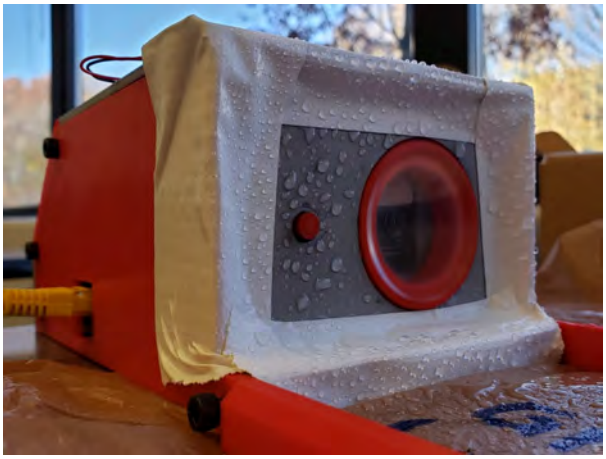

(c) Lens is Spun for 10 Seconds

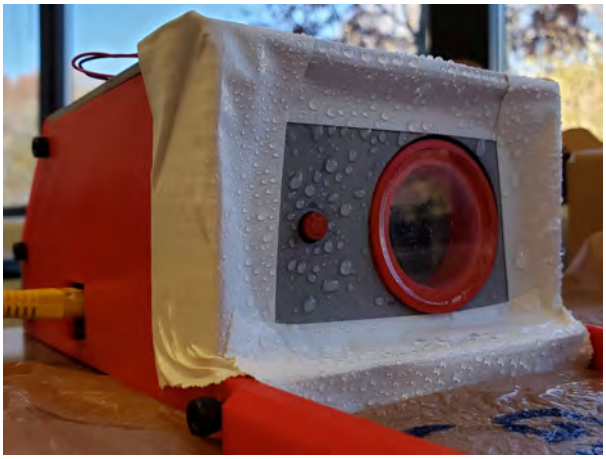

(d) Photo Taken of Cleared Lens.

Figure 6: A step by step procedure of how we tested the effectiveness of our soiling reduction system.

4.3 Stylistic Comparison

Testing of the visual appeal is a difficult task as it is based on how people react to the new design. Appeal is important as the design is supposed to be marketed to the public and, therefore, visual appearance must be taken into consideration. A question without implicit bias was asked and the participants response was recorded. An image of the previous design next to the our redesign was shown and the following question was asked:

"If you were to replace a mirror on a truck with a camera system, which one of these two designs

would you choose to replace the mirror?"

The poll was taken in multiple places, including three online platforms and in-person. Responses were recorded to compare the visual appeal between the two. *Figure 7* is the image that was used in the polling.

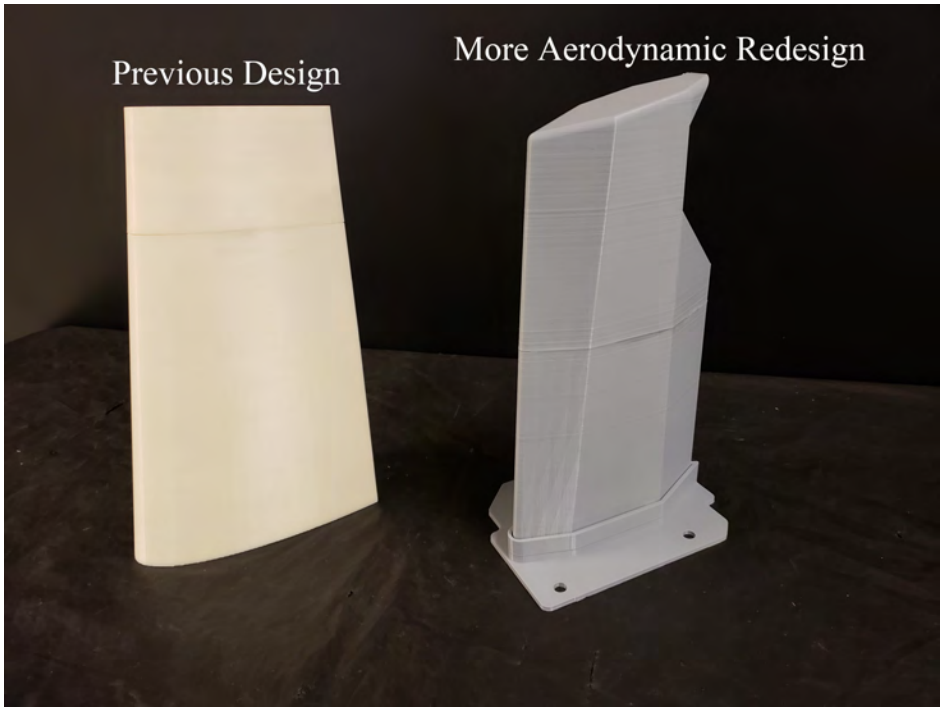

Figure 7: Photo of the old design and the more aerodynamic redesign from last year to this year.

5 Data Analysis

Details of the analysis conducted with the data acquired from our experiments are listed below. Numerical analysis is completed for the aerodynamics, soiling, and stylistic components, while also including analysis of the raw data. Conversion to a scalar, self-similar form is also detailed with a commentary on a combination of the raw data, the self-similar forms to the goals set for ourselves, and comparisons to the previous groups design.

5.1 Aerodynamics

Data was collected in order to study the aerodynamics of our model for the MirrorEye™ system. The details of how the raw data allowed us to achieve non-dimensional terms such as coefficient of drag, and Reynolds number are explicitly stated. In summary, we were able to **achieve and surpass our goal** of a 20% decrease in the drag coefficient.

We achieved a drag coefficient reduction from 0.55 to 0.32: a 42% reduction in the overall drag of the product. By reducing the size of the design, we were also able to lower the C_dA by 64% overall. C_dA, the metric of aerodynamic performance used by the previous research group, was decreased from 0.014m^2 to 0.005m^2.

5.1.1 Statistics

Ensuring that our acquired data was able to correctly model the aerodynamic design was crucial. As such, ample amounts of data were acquired for different cases at different moments in time. Data was taken to determine the best angle of attack of the design before more was collected at the optimal operating angle in order to achieve a satisfactory confidence interval in our testing.

- **Acceptable Confidence Interval:**

  A 95% confidence interval is the standard for most statistical analysis and is what we will use. The goal is to make this interval as small as possible without taking a redundant amount of data points in testing. The maximum z-score for a 95% confidence interval is 1.960, and multiplying this by 1.1 gives a value of 2.156, which is the z-score that we were aiming for in our statistical analysis.

- **Number of Data Points:**

  Getting to a z-score under 2.156 would require that we take 16 data points at each testing interval. This quantity of data points satisfied the balance between having a high number of data points and saving money through a reduction of time in the wind tunnel. Collection of 16 data points (8-40 m/s, in 8 m/s increments) netted us a z-score of 2.131 for a 95% confidence interval, which is only slightly less than the 2.156 threshold.

- **Displaying Values:**

  Our data will be displayed and communicated through the means and standard deviations of all data points. We will show variance of our data through the bounds of a 95% confidence interval.

5.1.2 Applicable Equations

Shown below are equations that we used to analyze the data and aid in our conclusions for the aerodynamic properties of our design.

- **Density:**

  The first step to characterize the flow requires us to determine the density of the air at the time of testing. The pressure of the wind tunnel and the temperature at the time of testing was collected regularly. The density was calculated from these two values using the ideal gas law equation in terms of density as shown by *Equation 1*.

$$\rho = \frac{P}{RT} \tag{1}$$

- **Drag:**

  The drag force is essential in evaluating our performance to meet our goals. A drag value from the wind tunnel testing was obtained and, from that, a calculated coefficient of drag value was formed for our conclusions. *Equation 2* shows the calculation used to find the drag coefficient.

$$D = \frac{\rho A V^2 C_D}{2} \tag{2}$$

- **Dynamic Viscosity:**

Dynamic viscosity determines how resistant a fluid is to movement, and is critical in the solving of Reynold's Number. The Sutherland equation, seen as *Equation 3*, inputs the temperature of the flow and returns the expected dynamic viscosity of air.

$$\mu = \frac{b T^{3/2}}{T + S} \tag{3}$$

- **Reynolds Number:**

  Reynolds number characterizes the ratio of inertial forces to viscous forces, and is proportional to velocity, which helps to characterize how our model behaves at varying speeds. This variable can be calculated using *Equation 4*.

$$Re = \frac{\mu L V}{\rho} \tag{4}$$

5.1.3 Aerodynamic Analysis

The study of the aerodynamic characteristics required the development of a method to convert our data into usable information. Such methods included developing calibration curves to determine the force loads on the transducers and using equations to determine key factors in order to non-dimensionalize the data.

- **Calibration:** The strain gauges located on the force balance in the wind tunnel generate a voltage proportional to the amount of force applied to them, which is then digitized as counts in the computer with an integer value of 1 to 4096. To calibrate, we applied a known force to the balance by hanging weights on the drag sensor and recorded the count values reported for that sensor by the computer. Linear regression was applied to the data. Once applied, the counts scaled linearly with the force applied to confirm the calibration worked as desired. A count per pound-force value was found and reentered into the computer. The drag force was then tared such that it read zero during static conditions. The computer can then translate the difference of the current count value from the baseline into a drag force reported in pound-force. This process was done every time the mount was altered significantly, e.g. between the MirrorEye prototype and the traditional mirror, and between different days of testing.

  After force balance calibration was completed, we ensured the prototype was set to 0° and flow was induced in the tunnel. A sweep of angles between -7° and +7° was used to find the angle with minimum drag. The angle was set at the minimum drag value (0°) and then further testing was completed.

- **Adjusted Values:**

  Our data produced values from the computer which had been pre-programmed to return a value for airspeed. In addition to this, we recorded the dynamic pressure as read from pressure taps located on the side of the 5' x 7' wind tunnel. This pressure was converted to velocity for the free stream flow in the wind tunnel to determine that the computer DAQ system was off by a factor of 1.15 when projecting velocities. The multiplication factor was used to correct our recordings for all airspeed data to accommodate for this difference.

- **Raw Data:**

  Analysis of raw data is vital in showing that it is following the expected pattern. Analyzing the data can give us ideas on trends that have formed during the data acquisition process. The base data also

provides general ideas on the performance of the design in real time. Raw data from the tested full-scale models in the 5' x 7' wind tunnel instantly showed the total reduction in the drag between the new design and the original mirror before any data analysis took place.

Data was acquired in two separate sets. One set was a general characterization of the data where we acquired data for different situations including mounting angles, initial C_D characterization, and data for the standard mirror in order to compare to the previous years experiments, to ensure their validity. The second iteration was solely to get more precise and accurate characterization of our system. We ran at variable angles to find the angle of lowest drag, which would be the primary operating condition. Five times the amount of data from the initial set was collected to get a better characterization of our system at operation condition. In *Appendix A.4*, the data for both test sets is listed. A plateauing of the values can be seen between each test at independent velocities which shows that the data is consistent across measurements, indicating no hysteresis.

- **Trends in Data:**

  The data was compressed down into the averages at each velocity and changed to SI units for ease of use, which displayed the expected analytical trends in the system. We expect the drag on the system to quadratically increase as the free stream velocity increases. As seen in *Figure 8*, the trends that we expected are shown. It can be observed that as speed increases the value of the drag increases from about 1 N of force at 8 m/s (20 mph) to 6 N at 43 m/s (90 mph).

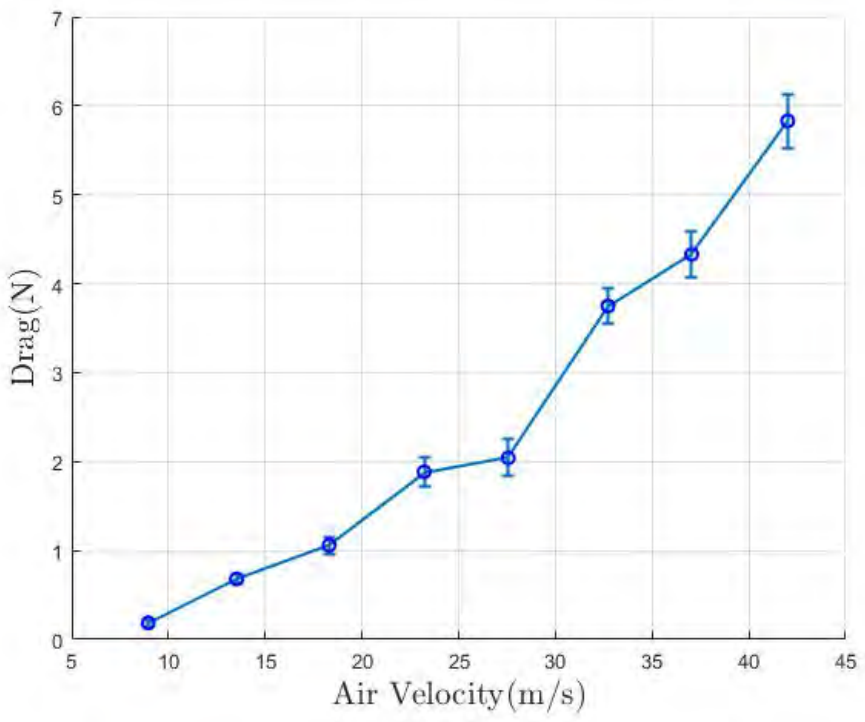

Figure 8: Showing the drag that the new design produces between 8 m/s (20 mph) to 43 m/s (90 mph) in Newtons. The error bars display the 95% confidence interval.

The data that we acquired for the original truck mirror was compared to the data collected last year to validate their numbers. From this we were able to get a readout of the original mirror alone and

compare to the data they had last year. Our data, seen in *Figure 9a*, nets us a C_DA of around $0.11m^2$. Analyzing the data that they had last year, seen in *Figure 9b*, our C_DA falls in their relative range between 0° and 15° angle of attack.

Therefore, we can expect that their data is valid for comparison to our experimental results. However, we are limited due to their data display not having all values available. As such, we can only display values of C_D as last year they focused on displaying C_DA instead.

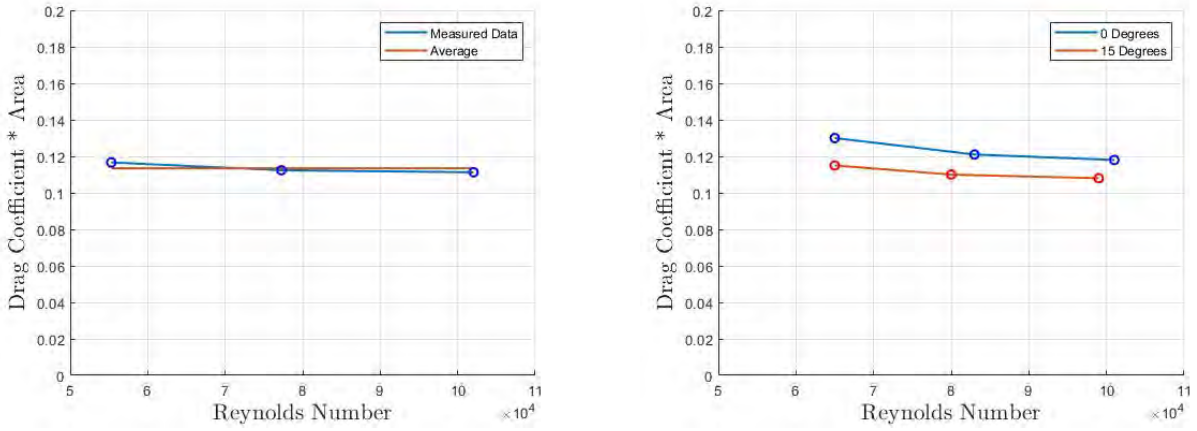

(a) Our collected data on standard truck mirror.

(b) Last years data on standard truck mirror[4].

Figure 9: Data comparison of the standard mirror to determine if we can compare our new design data to last years design data.

5.1.4 Aerodynamic Results

Using the acquired data and established trends, we can characterize the flow around the redesign of the MirrorEye™ camera system. The first step would be to translate these results into a non-dimensional form that only depends on the geometry of the design and no other variables including size, air speed, or density. The data was converted to a non-dimensional form that involved changing the drag into a coefficient. C_D was found using the known flow properties and the size of the planform area, which in our case was the frontal area of the model. Seen in *Figure 10a* we can see the conversion from drag to C_D still related to air speed in m/s. The second part of the analysis is to convert the flow speed into a Reynolds number to be able to apply the non-dimensionality at any flow speed for any atmospheric condition. The collected flow properties are used again to produce the Reynolds number for each case, seen in *Figure 10b* is the relationship between C_D and Reynolds number.

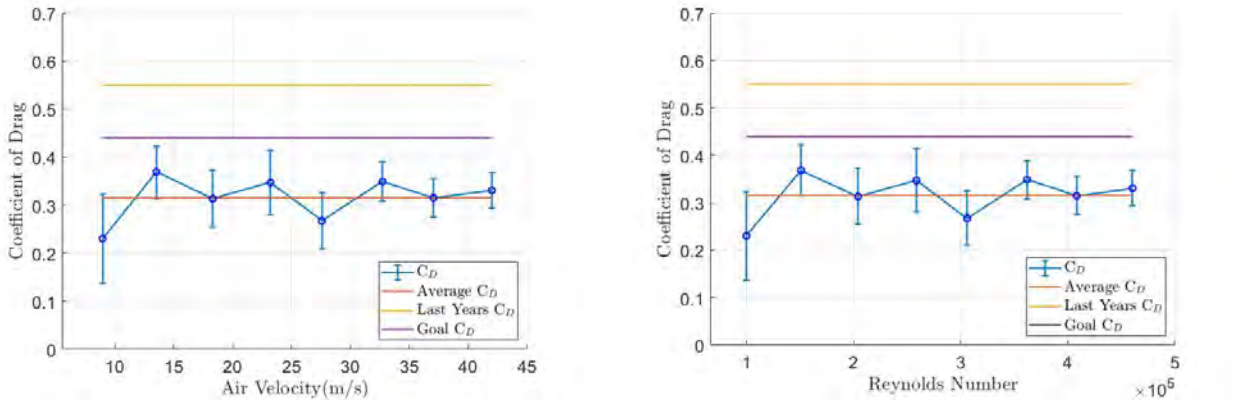

(a) Coefficient of drag as function of airspeed

(b) Coefficient of drag as function of Reynolds Number

Figure 10: Coefficient of drag plots based on free stream velocity, or Reynolds number at 29.36 inHg and 40 °F. Shown is the C_D from last year, our goal C_D, and our average C_D, all of which are displayed with error bars showing a 95% confidence interval.

Seen in *Figure 10a* and *10b* is the averaged values of the C_D. We ultimately obtained a drag coefficient value of 0.32, a reduction of 42%, on our final MirrorEye™ model. This meets our goal of a 20% reduction in the coefficient of drag from the previous model of 0.55 which is also displayed on the figures.

Since results were validated from the previous group in this paper by comparing our mirror test to their mirror test, we also wanted to probe into how it performed to their design specifications. They produced results in C_DA form instead of just C_D. Their results showed a reduction from the current production MirrorEye™ at 0.021 m^2 C_DA to a C_DA of 0.014 m^2 for their proposed design. A reduction that corresponds to a 33% decrease. Our proposed design surpasses their design and has a C_DA of 0.005 m^2, a 64% reduction from their proposed model and a 76% reduction from the production model. An important note is that this reduction is also partially due to the fact that our design is slightly smaller in geometric size from last year's model; however, even if our model increased to the same frontal area size as last year's, it would still net a 42% reduction in the C_DA.

5.2 Soiling Reduction

Data was collected through various testing schemes and procedures in an effort to reduce soiling of the MirrorEye™ camera lens as much as possible. The details and results of this testing can be seen in this section with a highlight on the image analysis performed using images obtained through the custom testing apparatus.

5.2.1 Statistics

We wanted to ensure that our data would correctly represent results in reality. To make certain of this, we aimed at finding the 95% confidence interval to match what was done in terms of the aerodynamic optimization. Sixteen data points were again taken to warrant a 2.131 z-score for the no hydrophobic material tests. On the other hand, due to moisture creeping in behind the lens, we had to halt testing at 11 trials for the hydrophobic material tests, which indicated a modified z-score of 2.228. We recognize this is not ideal; however, we remain confident the data represents the systems performance in both cases. The performance of the system exposed to a systematic soiling of the lens enabled valid image collection for later data analysis.

5.2.2 Applicable Equations

- **Average Difference Equation**

  Equation 5 is the main equation used for the analysis in our soiling reduction system. The following allows for a comparison between two different images, a necessity for the analysis of our system. The images are represented as matrices where each pixel is a value in a matrix. The images used in this equation have been converted from RGB to gray-scale in order to keep the image matrix one dimensional.

$$AD = \frac{\Sigma_{i=1}^{M}\Sigma_{j=1}^{M}|X(i,j) - Y(i,j)|}{M \times N} \tag{5}$$

  where:

  - X(i,j) represents the original image
  - Y(i,j) represents the blurred image
  - and M $\times$ N is the resolution of the images

- **Normalization**

  In order to view the images objectively based upon the values given, we must normalize the intensity levels given in our average difference equation as the range for a gray-scale pixel value is from 0-255. The normalization of the difference matrix can be calculated using *Equation 6*.

$$AD_{normalized} = \frac{AD}{255} \tag{6}$$

- **Blurriness Percentage**

  The normalized average difference values of the images can be used to determine the percent-reduction in blurriness after our soiling reduction system had been activated with the lens spinning for ten seconds. This relationship is shown in *Equation 7*. Once again, this is a matrix math equation that divides two matrices containing information about the average difference between two images.

$$\%\ Reduction = [1 - \frac{AD_{Normalized,PostSpin}(i,j)}{AD_{Normalized,Soiled}(i,j)}] \times 100 \tag{7}$$

5.2.3 Soiling Analysis

To determine how well the soiling reduction system operated, we developed an image analysis program that compares images taken by our camera located in the testing apparatus. We chose to use MATLAB to perform our analysis, as MATLAB has a large library of built in image analysis tooling, as well as appropriate functionality with Raspberry Pi boards. MATLAB also allows for easy interpretation of matrix math equations, such as the ones discussed in the above section.

The developed program functions by taking an input of images from our testing apparatus camera and separating them into three categories. The categories correspond to the stage of the testing sequence at which they were taken. This organizational pattern enables us to accurately begin with a valid control image for every test iteration. The categories are as follows:

- Baseline: image taken with no soiling on the lens, pre-activation of the soiling reduction system

- Soiled: image taken after a sufficient amount of soiling has been applied to the lens
- Post-Activation: image taken after our soiling reduction system has operated to remove soiling on the lens

These images are input into the analysis function that compares the blurriness between the different images by computing the average difference between the the three categories as shown by *Equation 5*. The soiling reduction percentage produces an accurate and simple method to calculate the blurriness of the image, as shown by a study completed at the Multimedia University in Malaysia [5]. The total data set that was input into the analysis program consisted of over 200 images. The image analysis code can be found in *Appendix A.2.1*.

(a) 3rd Person Base Image

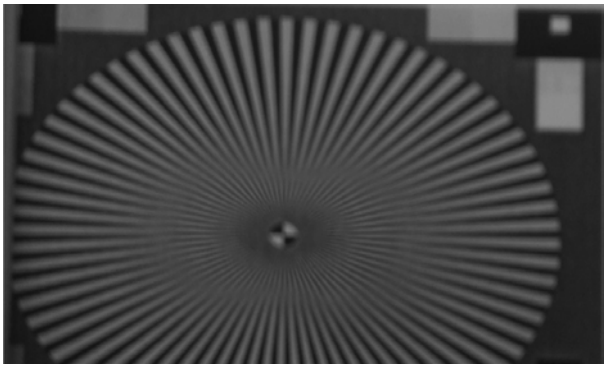

(b) 1st Person Base Image

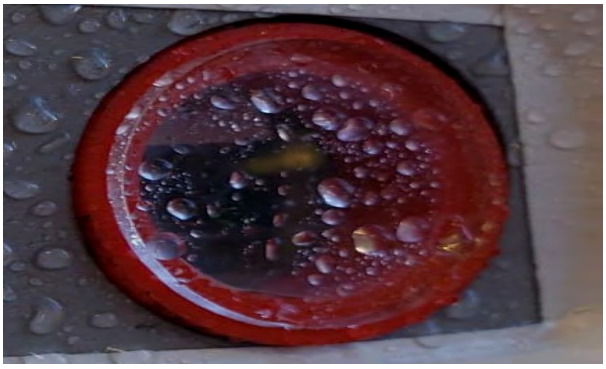

(c) 3rd Person Soiled Image

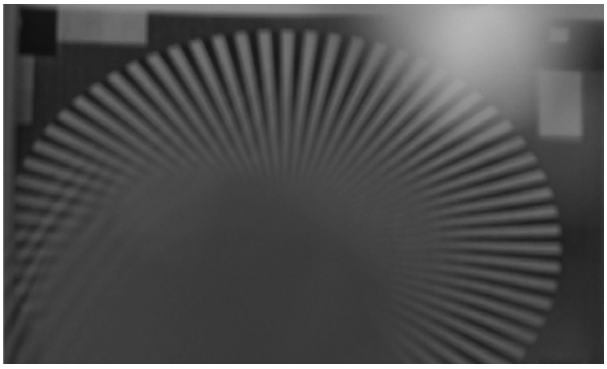

(d) 1st Person Soiled Image

(e) 3rd Person Post-Activation Image

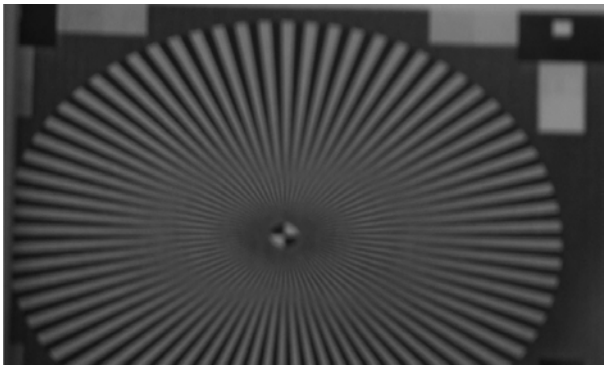

(f) 1st Person Post-Activation Image

Figure 11: Comparison of lens [left] and camera feed [right] during testing sequence where camera feed images are used in image analysis algorithm.

Figure 11 shows examples of the type of 200 images captured during the testing sequence that were used in the analysis of the overall data. The images showcase the base, soiled, and post-activation of the soiling reduction system through a 1st and 3rd person view point.

5.2.4 Soiling Analysis Results

The following results were formed using the image analysis program developed in MATLAB to calculate the difference in blurriness of an image during the soiling reduction testing sequence. The figures indicate a positive reduction percentage for all cases, which matches observations made by our group during testing of lenses with both hydrophobic and non-hydrophobic application.

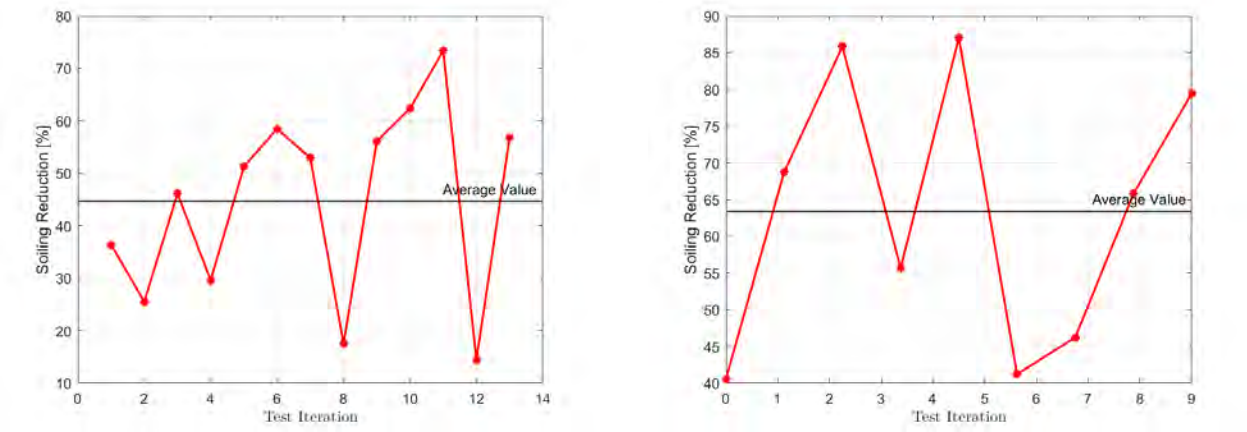

(a) Soiling reduction % for test sequence with no salt and no hydrophobic material

(b) Soiling reduction % for test sequence with no salt and hydrophobic material

Figure 12: Plots showing the analysis algorithm's results from the soiling reduction testing.

Figure 12 features two plots displaying the average reduction of soiling corresponding to:

- Soiling reduction system with no hydrophobic application: 45% average reduction
- Soiling reduction system with hydrophobic application: 63% average reduction

The soiling reduction percentage was not calculated as a function of revolution rate of the spinning lens due to inconsistencies in the revolutions of the lens. The poor quality of the motor used and uncollected frictional and vibrational forces contributed to this limitation. For our analysis results, we omitted the testing done with the salt water mixture as the differences in soiling reduction were less than 1% of our values received for the regular water tests. The omission showcases a need for further exploration into different soiling types in the future. However, we believe the results obtained are reflective of the ability of the test apparatus to remove soiling on a camera lens when either water is used or the tested salt water dilution is exposed to the lens.

	W/O Hydrophobic Material	W/ Hydrophobic Material
Avg. Soiling Reduction	44.7 %	63.4 %
Standard Deviation	± 18.3 %	± 18.4 %

Table 1: Summarized soiling reduction values obtained from testing.

The large standard deviation values are due to inconsistencies in the testing sequence, such as lighting, the vibration of the soiling reduction system, and our difficultly in having a reproducible method of applying the soiling to the lens. The combination of these factors can produce inaccurate intensity values in our images when read into MATLAB, and can then produce error in our average difference calculation and analysis. With that being said, it is important to note that even accounting for average soiling reduction with a plus/minus of the standard deviation results in a consistent net positive clearing of the lens on the camera system, achieving our goal.

5.3 Stylistic Comparisons

From our four separate polling methods, we acquired a moderate amount of responses from engineers and non-engineers alike. *Figure 13* shows the results of our poll and what the distribution was for each of the designs. The graph clearly shows that there is a substantial number of answers for both choices; however, the design we produced did receive proportionally more positive response and was therefore selected more often. We believe that, if marketed correctly, our product would surpass the sales of the previous design based solely on aesthetics and thus would be more competitive in the market.

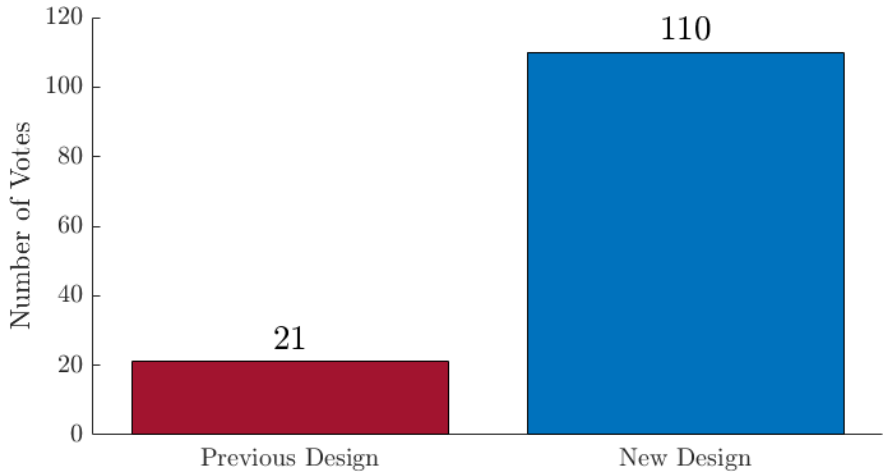

Figure 13: The selection between the two designs described in Figure 7 showing the proportion of each result type and the overall totals for both designs.

6 Alternatives, Omissions & Limitations

Below are alternatives that could be or were briefly explored, omissions to our data collection that may have marginally altered the results, and some limitations to our work that we would have further pursued had we not been limited by time or featured a more specialized and sufficient background in the area.

6.1 Alternatives

Through our process of designing both systems, we came up with a few more ideas that were explored briefly in terms of their feasibility of effectiveness. We produced ten unique designs that could have used as our new final redesign and ran them through Star-CCM+ CFD simulations to get a general classification. The preliminary tests revealed each had its own upside including smaller frontal areas, good aerodynamic properties, and different artistic ideas. For the sake of time, we reduced it down to a single design, while no longer considering the other nine designs. The final design was also modified by changing the fillets to larger radii. This change had variable performance changes in the CFD analysis; however, these changes either had negative impacts or less than 1% drag decreases to the overall design. The geometric changes made the design look less appealing stylistically, so the decision was made to stick with the original redesign.

In terms of soiling, we looked into the application of using a pressurized air system that would blow across the lens in order to clean it, but we were limited by time and resources and decided to focus on the singular soiling reduction technique that was the design incorporating a spinning lens.

6.2 Omissions

Given the design of our soiling reduction apparatus and time restrictions, we were not able to fully combine the apparatus with the redesigned MirrorEye™ model. Combining the two would allow for the testing of the coupled soiling and aerodynamics portions into a single system, which could be tested in the wind tunnel. This is important as the camera system would not be exposed to direct exposure of the elements in operation.

Different types of debris beyond those mentioned were not tested to expose the lens to alternate soiling culprits. We also did not attach the enhanced aerodynamic model to a vehicle in order to see the impact our system would have. This was due to both time restrictions and also not having access to a large truck for testing purposes.

6.3 Limitations

Time has been the major limiting factor in our design choices, from only pursuing one design in-depth for aerodynamic optimization, to only being able to test one system for the soiling reduction apparatus. We have hypothesized techniques such as making the current soiling reduction automatically activated through the use of sensors that are triggered when debris is present on the lens, to machine learning that can determine when the lens is soiled. Due to restrictions in time, as well as gaps in knowledge, these high level applications could not be pursued further at this time.

7 Conclusion

The two systems that were developed both operate as hypothesized. Both are able to meet the goals set forth and we were able to produce a design that fulfilled the specifications for what was required. The aerodynamic system was able to reduce the C_D by 42% compared to last year's design, while offering a stylistic design similar to the current MirrorEye™ system. Because of this, our system offers a design, independent of size, that can be implemented on vehicles of all shapes and sizes to offer an overall better performance to the customer to that of the traditional MirrorEye™ camera system. This ensures an even greater returns on investment to customers that purchase this to replace their traditional side mirrors.

The additional system for addressing soiling also offers improvements to the camera system to make it a safer and more effective to use overall. With proper implementation of soiling reduction with similar

behavior to that tested in this project, MirrorEye™ camera systems would be able to be used without the constant problem of the system becoming unusable or unsafe for use by customers due to soiling. In all, the ideas and designs tested in this report offer a solution to the problems presented, while offering a product that can be implemented as the next iteration of MirrorEye™ camera systems. We fully recommend the use of the aerodynamically optimized MirrorEye™ camera system redesign to offer an even more cost effective, safe, and stylish system with room for expansion into soiling reduction techniques using the discussed developmental technology.

8 Future Efforts

Even with the vast improvements that have already been made, there is still room for further expansion in the project. Although we believe we have reached the point of diminishing returns for improving upon the aerodynamics of the system, there are some novel ideas we did not have the time to pursue during this project with regards to the soiling reduction system.

8.1 Self-Activation

The idea to implement some sort of self-activating soiling reduction system could be completed in multiple ways. A sub-system would need to be installed that would automatically spin the motors to activate our primary soiling reduction system in the case of the lens becoming soiled. Possible solutions to this problem are listed below with varying levels of difficulty.

- **Artificial Intelligence:**

  AI could be used to trigger the soiling reduction system by implementing an algorithm that can recognize when debris has accumulated on the lens using machine learning to understand what it means for an image to be clear and unobstructed. This method would be high difficulty and costly to implement in terms of software development and image recognition.

- **Trigger using Image Analysis Algorithm:**

  The image analysis algorithm detailed in this report could aid in the implementation of a program to run the motor when the analysis shows the image has reached a certain blurriness percentage. A limitation with this method would be the amount of data that must be processed rapidly.

- **Infrared Sensor (IR):**

  Taking a note from the automotive industry in regards to using IR sensors to automatically activate windshield wipers, an implementation could be made with the soiling reduction system. It is possible this could be the easiest method in regard to automatic soiling reduction.

8.2 Full System Integration

The integration of the soiling reduction system into the redesigned camera model would create one cohesive unit. The result would be an entire MirrorEye™ prototype system capable of direct comparison with the actual MirrorEye™ system. The prototype could be tested in the wind tunnel to observe the coupled relationship between the soiling reduction system and flow around the model. Such an effort could lead to other areas to improve upon such as: improved image quality, integration with the vehicle software, and driver-system interactions with the system.

8.3 Soiling Reduction Testing Methods

The final area we would have liked to have touched upon, would have been the exploration of testing new and different materials and their application methods for the soiling of our soiling reduction sub-system. This would result in having a more standardized method of soiling the lens.

8.4 Image Transformation and Vibration Dampening

During the testing for soiling characterization, there were difficulties in performance due to vibrations caused by the motor located within the testing apparatus. A vibration induced to our system would slightly shift the camera around, making image analysis much more difficult. Adding more reliable vibration dampening would make testing more efficient and possibly provide improved results.

There was also an attempt during image analysis to perform an image transformation, which would automatically account for the translation imposed on the images by the vibration by translating the images to match an exact specified frame. This specified frame would align all the images to the exact same location to ensure only the blurriness was being measured using the average difference equation, instead of accounting for blurriness and potential image translation caused by vibrations. This method was briefly explored and the MATLAB code can be seen in the *Appendix A.2.2*.

9 Project Costs

The cost of the MirrorEye™ camera system optimization can be seen below in *Table 2*. The vast majority of the cost was concentrated in labor costs, while the second largest costs come from the use of the facilities. The cost of materials was $256, which is $144 under the budget we were restricted to in regards to materials.

Category	**Item**	**Unit Cost ($)**	**Units**	**Costs ($)**
Labor	Engineers	40 per Hour	650	26,000.
			Subtotal	26,000.
Facilities	5’ x 7’ Wind Tunnel	315 per Hour	12	3,780.
	2’ x 2’ Wind Tunnel	60 per Hour	2	120.
			Subtotal	3900.
Materials	Printer Filament	20 per Roll	2	40.
	Plexiglass	30 per Sheet	1	30.
	Electronics	138 per System	1	138.
	Misc	48 per Set	1	48.
			Subtotal	256.
Total				30,156.
Overhead		50% of Total		15,078.
Grand Total				45,234.

Table 2: All Eyes on MirrorEye™ Cost Table

10 Project Schedule

To help us remain on schedule and keep important deadlines in mind, a Gantt organizational chart was created to guide us. The chart includes all of the major milestones and developments, as well as their respective completion times. The chart made sure to give us a buffer time of about a week from the final deadline in order to provide the team with more time in case of extraneous circumstances. We managed to finish our testing earlier than anticipated and completed all of our data gathering and analysis prior to the end date of the project.

Figure 14: Project Schedule, deadline, and completed work

References

[1] W. Riley Garrott, M. A. F., and Mazzae, E. N., "Hardware Evaluation of Heavy Truck Side and Rear Object Detection Systems," *National Highway Traffic Safety Administration*, 1995.

[2] "International Energy Outlook 2016," *U.S. Energy Information Administration*, Vol. pp. 127-137, 2016.

[3] "Clear view screen," *Wikipedia*, 2005.

[4] Andrew Cox, A. L. F. S. J. V., Jordan Howie, "Final Report: Aerodynamic and Soiling Study for Stoneridge MirrorEye™ System," *University of Michigan*, 2019.

[5] Mahmoud Elsayed, A. H. A. A. H. B., Fawaz Sammani, "A New Method for Full Reference Image Blur Measure," *Multimedia University*, 2011.

[6] "Sof Sole Heavy-Duty Waterproofer," *Dicks Sporting Goods*, 2019.

A Appendix

The following includes information that we have deemed too detailed for the main section report. However, we feel compelled to provide this information in hopes to provide help to future groups looking to work on our proposed future efforts.

A.1 CAD Model of MirrorEye™ Redesign

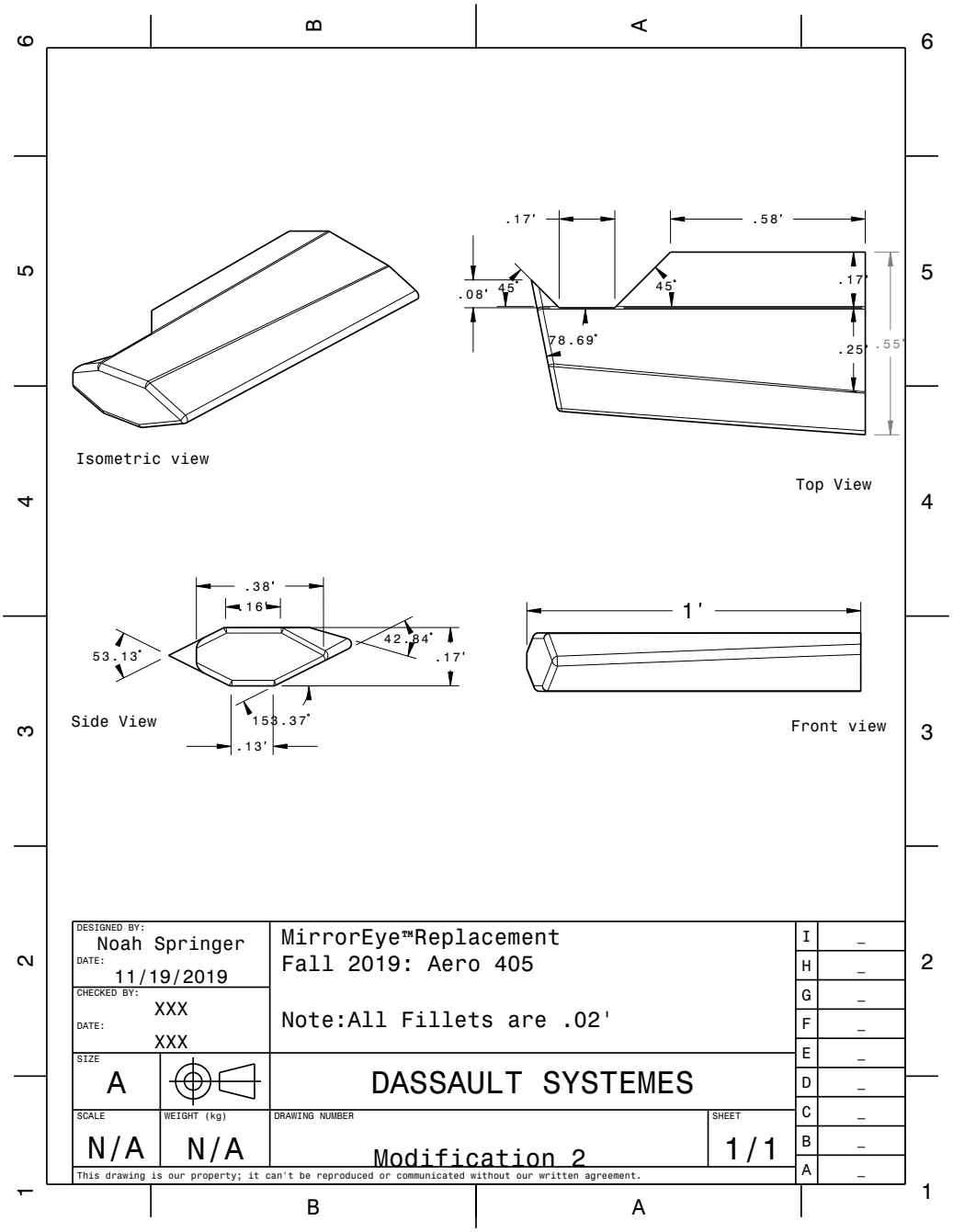

Figure 15: Dimensional model of MirrorEye™ camera system redesign

A.2 Analysis Programming

Even though code is usually not meant to be included in formal reports, we have included MATLAB code that we believe could be helpful for future efforts by other project teams. We believe the inclusion of code in this circumstance will provide the next team with a valuable resource as they continue the project.

A.2.1 Image Analysis Code

The following code was created in MATLAB with a purpose to read in a large set of images stored with specific names and perform image difference analysis. The analysis ultimately determines the percentage of blurriness of the input images using a comparison of images from pre-activation and post-activation of the soiling reduction test apparatus to an initial baseline non-soiled state.

```
%Andrew Caulkins
%MirrorEye – AERO 405
%ClearView Lens Image Analysis
%_____________________________________________________________________

clc
clear
close all

%% Reading in Images to Usable Data:
%Setting Variables:
count = 0;
for i=1:15
    for j=1:4
    Images{i,j} = imread(sprintf('SR_%d_%d.png',i,j));
    end
end

for i=1:9
    for j=1:4
    Images_Salt{i,j} = imread(sprintf('SaltR_%d_%d.png',i,j));
    end
end

for i=1:9
    for j=1:4
    Images_Hydro{i,j} = imread(sprintf('Hydro_SR_%d_%d.png',i,j));
    end
end

for i=1:9
    for j=1:4
    Images_Hydro_Salt{i,j} = imread(sprintf('Hydro_SaltR_%d_%d.png',i,j));
    end
end
%Separating Data into usable indices:
Base = Images(:,1);
Soiled = Images(:,2);
PostSpin = Images(:,3);

Base_Salt = Images_Salt(:,1);
Soiled_Salt = Images_Salt(:,2);
```

```
PostSpin_Salt = Images_Salt(:,3);

Base_Hydro = Images_Hydro(:,1);
Soiled_Hydro = Images_Hydro(:,2);
PostSpin_Hydro = Images_Hydro(:,3);

Base_Hydro_Salt = Images_Hydro_Salt(:,1);
Soiled_Hydro_Salt = Images_Hydro_Salt(:,2);
PostSpin_Hydro_Salt = Images_Hydro_Salt(:,3);

%% Computing Difference in No Salt, No Hydrophobic Material Soiling:
for i=1:15

    %Computing Difference in intensity from images:
    I_1{i} = abs(Base{i} - Base{i});
    I_2{i} = abs(Base{i} - Soiled{i});
    I_3{i} = abs(Base{i} - PostSpin{i});

    %Determining Average Difference:
    BlurrNormal(i) = mean(mean(I_1{i}))/255;
    Blurr_Baseline(i) = mean(mean(I_2{i}))/255;
    Blurr_Final(i) = mean(mean(I_3{i}))/255;

    %Percentage Difference:
    Diff(i) = (1 - Blurr_Final(i)/Blurr_Baseline(i))*100;
end

%% Computing Difference in No Salt, WITH Hydrophobic Material Soiling:
for i=1:9

    %% Average Difference:
    %Computing Difference in intensity from images:
    I_1_Hydro{i} = abs(Base_Hydro{i} - Base_Hydro{i});
    I_2_Hydro{i} = abs(Base_Hydro{i} - Soiled_Hydro{i});
    I_3_Hydro{i} = abs(Base_Hydro{i} - PostSpin_Hydro{i});

    %Determining Average Difference:
    BlurrNormal_Hydro(i) = mean(mean(I_1_Hydro{i}))/255;
    Blurr_Baseline_Hydro(i) = mean(mean(I_2_Hydro{i}))/255;
    Blurr_Final_Hydro(i) = mean(mean(I_3_Hydro{i}))/255;

    %Percentage Difference:
    Diff_Hydro(i) = (1 - Blurr_Final_Hydro(i)/Blurr_Baseline_Hydro(i))*100;
end

%% Computing Difference in Salt, no Hydrophobic Material Soiling:
for i=1:9

    %% Average Difference:
    %Computing Difference in intensity from images:
    I_1_Salt{i} = abs(Base_Salt{i} - Base_Salt{i});
    I_2_Salt{i} = abs(Base_Salt{i} - Soiled_Salt{i});
    I_3_Salt{i} = abs(Base_Salt{i} - PostSpin_Salt{i});

    %Determining Average Difference:
    BlurrNormal_Salt(i) = mean(mean(I_1_Salt{i}))/255;
    Blurr_Baseline_Salt(i) = mean(mean(I_2_Salt{i}))/255;
    Blurr_Final_Salt(i) = mean(mean(I_3_Salt{i}))/255;

```

```
102     %Percentage Difference:
103     Diff_Salt(i) = (1 - Blurr_Final_Salt(i)/Blurr_Baseline_Salt(i))*100;
104 end
105
106 %% Computing Difference in Salt, WITH Hydrophobic Material Soiling:
107 for i=1:9
108
109     %% Average Difference:
110     %Computing Difference in intensity from images:
111     I_1_Salt_Hydro{i} = abs(Base_Hydro_Salt{i} - Base_Hydro_Salt{i});
112     I_2_Salt_Hydro{i} = abs(Base_Hydro_Salt{i} - Soiled_Hydro_Salt{i});
113     I_3_Salt_Hydro{i} = abs(Base_Hydro_Salt{i} - PostSpin_Hydro_Salt{i});
114
115     %Determining Average Difference:
116     BlurrNormal_Salt_Hydro(i) = mean(mean(I_1_Salt_Hydro{i}))/255;
117     Blurr_Baseline_Salt_Hydro(i) = mean(mean(I_2_Salt_Hydro{i}))/255;
118     Blurr_Final_Salt_Hydro(i) = mean(mean(I_3_Salt_Hydro{i}))/255;
119
120     %Percentage Difference:
121     Diff_Salt_Hydro(i) = (1 - Blurr_Final_Salt_Hydro(i)/Blurr_Baseline_Salt_Hydro(i
        ))*100;
122 end
123
124 %Omitting bad data points:
125 Diff(3) = [];
126 Diff(10) = [];
127 Diff_Salt(6) = [];
128 %Printing Results:
129 Average_NoSalt_NoHydrophobic = mean(Diff)
130 Average_NoSalt_WithHydrophobic = mean(Diff_Hydro)
131 Average_Salt_NoHydrophobic = mean(Diff_Salt)
132 Average_Salt_WithHydrophobic = mean(Diff_Salt_Hydro)
133
134 %% Plotting Results:
135 X = linspace(1,13,13);
136 X_Hydro = linspace(0,9,9);
137 X_Salt = linspace(1,8,8);
138 figure(1)
139 plot(X,Diff,'-r*')
140 title('Water With No Hydrophobic Material')
141 xlabel('Test Iteration')
142 ylabel('De-Soiling [percentage]')
143 yline(Average_NoSalt_NoHydrophobic,'-b','Average Value' )
144 figure(2)
145 plot(X_Hydro,Diff_Hydro,'-r*')
146 title('Water WITH Hydrophobic Material')
147 xlabel('Test Iteration')
148 ylabel('De-Soiling [percentage]')
149 yline(Average_NoSalt_WithHydrophobic,'-b','Average Value')
150 figure(3)
151 plot(X_Salt,Diff_Salt,'-r*')
152 title('Salt-Water With No Hydrophobic Material')
153 xlabel('Test Iteration')
154 ylabel('De-Soiling [percentage]')
```

A.2.2 Image Transformation

In order to account for the vibration in the system, we have developed a prototype MATLAB program that uses a maximally stable extremal regions, MSER, feature finding algorithm in order to select a common region between a set of images and then cuts out a specified image around that region.

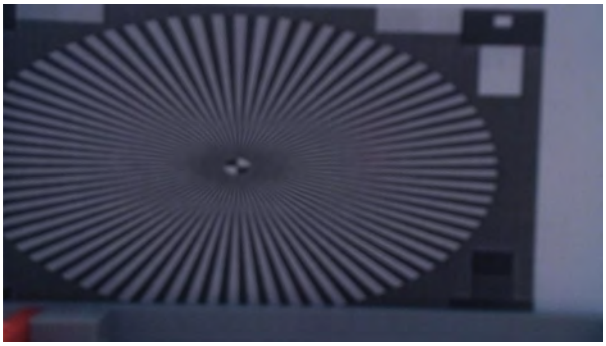

(a) Shifted Base Image

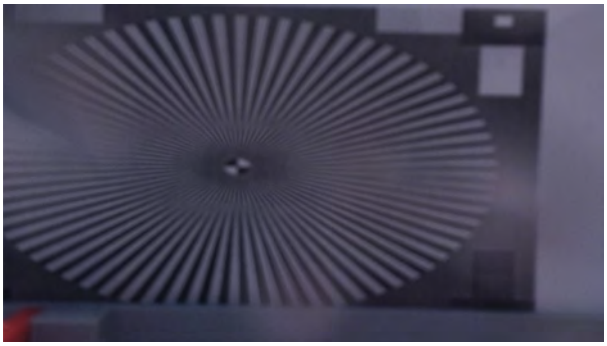

(b) Shifted Soiled Image

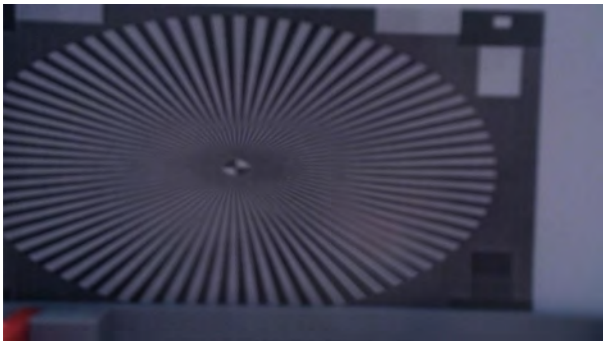

(c) Shifted Post-Activation Image

Figure 16: Example set of images used for our image transformation script featuring slight translation due to vibration.

As shown by this example set in *Figure 16*, the images are slightly translated. Specifically between *Figure 16a* and *16c*, corresponding to before and after activation of the motor. The same images are shown in *Figure 17*, but converted to gray-scale and run through the image transformation program.

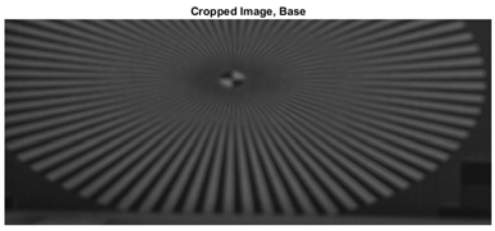

(a) Transformed Base Image

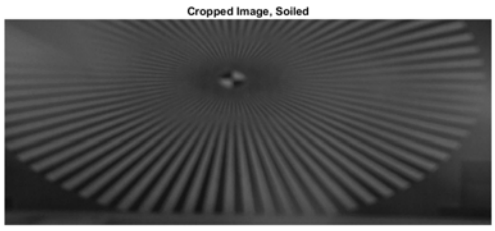

(b) Transformed Soiled Image

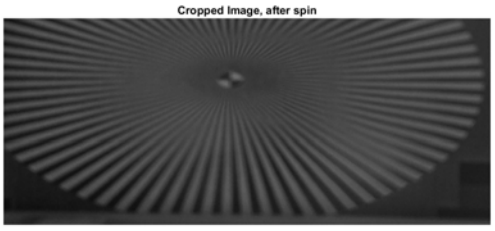

(c) Transformed Post-Activation Image

Figure 17: Example set of images processed with image transformation script.

Figure 17 displays the images after being processed in the prototype MATLAB program. The shifting of the images is partially corrected and the regular image analysis can now be ran on these modified images.

The code for this process is shown below and allows the user to specify where to crop out a portion of this image, starting at a specific feature. Current feature location is found at the point in the code where the max value of the image is located. The script then defines and crops the region based on that feature. This allows all images centered at a specific spot, even after some vibration offset the camera.

```
%Andrew Caulkins
%MirrorEye – AERO 405
%Image Isolation and Extraction
%_____________________________________________________________________

clc
clear
close all

%% Reading in Data:
I_11 = imread('SALTR11_1.png');
I_11 = rgb2gray(I_11);

I_12 = imread('SALTR11_2.png');
I_12 = rgb2gray(I_12);


I_13 = imread('SALTR11_3.png');
I_13 = rgb2gray(I_13);

%% MSER Features:
%Using the MSER Algorithm to determine key points:
```

```
regions_1 = detectMSERFeatures(I_11);
[features_1, valid_points_1] = extractFeatures(I_11,regions_1,'Upright',true);


regions_2 = detectMSERFeatures(I_12);
[features_2, valid_points_2] = extractFeatures(I_12,regions_2,'Upright',true);

regions_3 = detectMSERFeatures(I_13);
[features_3, valid_points_3] = extractFeatures(I_13,regions_3,'Upright',true);

%Isolating the key point we want:
%NOTE: THIS BELOW STEP NEEDS TO BE CHANGED.  THIS DOES NOT GIVE THE POINT
%ISOLATED SHAPE WE WANT EVERY TIME; THINKING WE NEED TO SEPERATE THE X AND
%Y COMPONENTS OF THE PIXELS INTO SEPERATE VECTORS, AND THEN FIND THE MAX OF
%THE X COMPONENT VECTOR, AND THE MIN OF THE Y COMPONENT VECTOR!!!
X_1 = max(valid_points_1.Location);
X_2 = max(valid_points_2.Location);
X_3 = max(valid_points_3.Location);

%Finding the average value of these key points, and rounding:
X_avg = [(X_1(1) + X_2(1) + X_3(1))/3,(X_1(2) + X_2(2) + X_3(2))/2];
X_avg = round(X_avg);

%Cropping Images:
Cropped_1 = imcrop(I_11,[X_avg(1)-1000 X_avg(2) 1000 400]);
Cropped_2 = imcrop(I_12,[X_avg(1)-1000 X_avg(2) 1000 400]);
Cropped_3 = imcrop(I_13,[X_avg(1)-1000 X_avg(2) 1000 400]);

%Plotting:
figure(1)
imshow(Cropped_1)
title('Cropped Image, Base')
figure(2)
imshow(Cropped_2)
title('Cropped Image, Soiled')
figure(3)
imshow(Cropped_3)
title('Cropped Image, after spin')
```

A.3 Hydrophobic Material Specifics

As predicted, application of a hydrophobic material on the camera lenses aided in soiling reduction. The material used to reach this conclusion was the Sof Sole Heavy-Duty Silicone Waterproofer, seen in *Figure 18*. This material is primarily used as a waterproofing application for combat and hiking boots and was purchased at a nearby sporting goods store in Ann Arbor. This material worked well for application on our camera lenses as it provided an invisible coat on the clear lenses and was able to exhibit better results in soiling reduction for our study.

Figure 18: Image of the hydrophobic material used for testing. [6]

A.4 Raw Data Matrices

Examples of the test matrices that we used during testing in *Tables* **??** *and 4*. These test matrices are what we used for the data collection of both the soiling reduction system and the aerodynamic efficiency system. Seen in *Table* **??** is the sample matrix for aerodynamic efficiency where we show the velocity of the system, the Reynolds number of the system, the drag, the standard deviation, and the 95% confidence interval. Seen in *Table 4* is the sample matrix for our soiling reduction system. The table shows the change in the amount soiling between each run and classifies the image name for proper use in MATLAB. Some data was removed for various iterations due to inconsistencies in the testing environment at the time of said iteration.

Temperature	Example (Degrees Celcius)		Pressure	Example (Pascals)		
Velocity (m/s)	Reynolds Number	Drag (Newtons)	Drag Standard Deviation	C_D (Unitless)	C_D Standard Deviation	C_D 95% Confidence Interval

Table 3: Aerodynamic Test Matrix

Test Iteration	No Hydrophobic Material [% Soiling Reduction]	With Hydrophobic Material [% Soiling Reduction]
1	36.3844	40.5801
2	25.5191	68.7409
3	46.1091	85.8185
4	29.5982	55.6704
5	51.2759	87.0138
6	58.4759	41.2111
7	52.9044	46.2198
8	17.5079	65.7907
9	56.0747	79.4418
10	62.3332	
11	73.3656	
12	14.4355	
13	56.7740	

Table 4: Soiling Reduction Test Matrix